Effect of Current on Transmembrane Potentials in Cultured Chick Heart Cells

NICK SPERELAKIS and D. LEHMKUHL

From the Department of Physiology, Western Reserve University School of Medicine, Cleveland

ABSTRACT By means of a DC bridge circuit one microelectrode was used for simultaneously passing current and recording transmembrane potentials. In some cells, depolarization increased the frequency of discharge whereas hyperpolarization decreased the frequency; the frequency/current relation was sigmoid. In other cells, polarizing currents were without effect upon frequency. The change in action potential magnitude was in proportion to the degree of polarization. From control values of about 5 mv/sec., the slope of the pacemaker potential increased to 60 mv/sec. upon depolarization and diminished to zero upon hyperpolarization. In many cells a transient hyperpolarization was produced on the cessation of depolarizing currents. The voltage/current relationship was linear and had a slope of about 13 MΩ. With an AC bridge circuit, the cell capacitance averaged 800 pf and the time constant, 9.6 msec. R_m was estimated to be 480 Ω-cm² and C_m, 20 μf/cm². The magnitudes of some prepotentials were affected by polarizing currents, which suggests that the prepotentials represent postsynaptic potentials.

It is now technically possible to record the transmembrane potentials of cultured heart cells (8, 11, 22). For example, we have recorded mean resting potentials of 59 mv and mean action potentials of 71 mv (22). Furthermore, the cells could be driven by intracellular or extracellular electrical stimulation with brief (<10 msec.) current pulses. The cultured myocardial cells are obviously similar in their electrophysiological properties to cells in intact hearts and hence represent a useful tool in the investigation of cell-to-cell interaction. An important advantage of the preparation is the relative simplicity with which one can interpret recorded potentials. The present study is concerned with the effect of current upon the transmembrane potentials of cultured chick heart cells.

ABBREVIATIONS USED IN THIS PAPER

V_m, ΔV_m, membrane potential (mv), change in membrane potential (mv).
V_p, $\dot{V}_p$, pacemaker potential (mv), slope of pacemaker potential (mv/sec.).
R_{cell}, R_m, cell resistance (MΩ), specific membrane resistance (Ω-cm²).
C_{cell}, C_m, cell capacitance (picofarads), specific membrane capacitance (microfarads/cm²).
T_m, membrane time constant (msec.).
$[Na^+]_i$, $[K^+]_i$, $[Cl^-]_i$, intracellular concentrations of Na^+, K^+, Cl^- (mM).
$[Na^+]_o$, $[K^+]_o$, $[Cl^-]_o$, extracellular concentrations of Na^+, K^+, Cl^- (mM).
E_{Na}, E_K, E_{Cl}, diffusion potentials for Na^+, K^+, Cl^- (mv).
g_{Na}, g_K, g_{Cl}, chord conductances for Na^+, K^+, Cl^- (mmhos/cm²).

METHODS

The tissue culture and electrophysiological techniques employed have been previously described (22). In brief, hearts from 6 to 8 day old chick embryos were dissected under sterile conditions. The atria were discarded and the ventricular cells dispersed by 0.1 per cent trypsin in Ca^{++}-free, Mg^{++}-free solution. The cells were cultured 1 to 7 days before experimentation. The incubation medium (pH 7.2) was a modified Puck's solution (30) containing horse serum, a synthetic nutrient medium, and antibiotics. The ionic composition of the medium in mM included: 144.7 Na^+, 4.5 K^+, 1.5 Ca^{++}, 0.8 Mg^{++}, 142 Cl^-, 9.7 HCO_3^-, 0.5 $H_2PO_4^-$, and 0.8 $SO_4^=$. After several hours in culture, most of the spherical cells became attached to the bottom of the dish and then became thin and elongated. Long, narrow processes often extended from the cell body and made contact with neighboring cells. Unless in contact, the rhythm of a cell was independent of its neighbors. With further growth, the single cells reassembled into groups, one cell thick, patterned as nets, rosettes, and sheets attached to the glass at many foci. Neighboring cells usually contracted synchronously but the activity of such local groups usually was not synchronized with that of the neighboring local groups. All studies were made on such reassembled cells; no correlation was made between the pattern of organization of the reassembled cells and whether the impaled cells were driven or non-driven. The culture dish was mounted on the stage of a microscope (total of × 600 with a × 40 reflecting objective lens) for visual observation of the cells and visual control of the movements of the microelectrode (de Fonbrune micromanipulator). The cells were maintained at 35°C during the impalements.

The capillary microelectrodes (flint glass) had tip diameters of about 0.5 μ, resistances of 15 to 50 megohms, and were filled with 3 M KCl. The reference electrode was an agar salt (Ringer) bridge immersed in the culture medium. Both electrodes were connected to calomel half-cells. The potentials were recorded with transistorized DC preamplifiers (electrometer-input, capacity neutralization) and a dual-beam cathode ray oscilloscope. By means of a bridge circuit (Fig. 1) a single microelectrode was used for passing current and for recording transmembrane potentials (12). The resistances of the microelectrode, calomel half-cells, bathing fluid, and cardiac cell

constituted leg *AB* of the bridge. The total non-cellular resistances of the bridge between points *A* and *C* were independently measured before impalement by the "ramp" method (*cf.* reference 23). A square-wave stimulator and a stimulus isolation unit (*S.I.U.*) were connected across the bridge at points *B* and *D*. Preamplifier *V* monitored the potential difference between points *A* and *C* and preamplifier *I*, that between points *E* and *C*. The input impedance of preamplifier *V* was reduced from about 10^{12} ohms to about 5.5×10^{8} ohms because of the shunting bridge resistances;

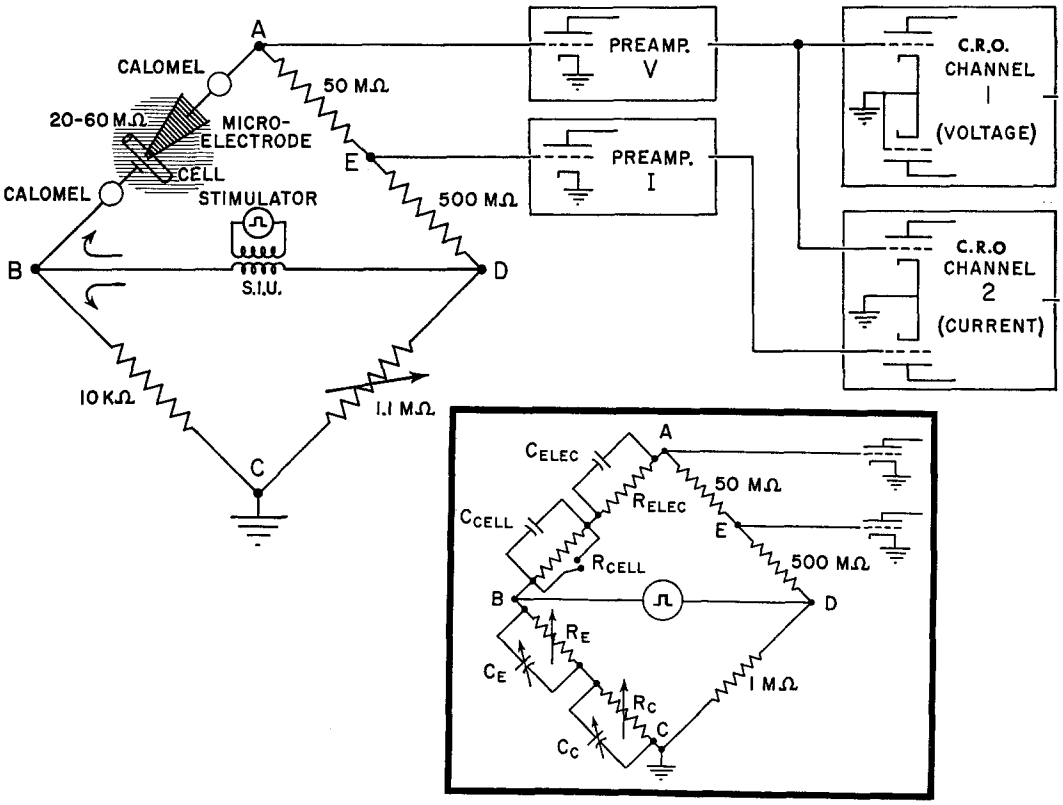

FIGURE 1. Schematic diagram of DC and AC bridge circuits and apparatus used to pass constant current pulses through the voltage-recording microelectrode, thus enabling one microelectrode to be used for simultaneously passing current and recording voltage. See explanation in text.

the current drawn from the cell electromotive force is only about 10^{-10} amp and the voltage measurements are underestimated by less than 10 per cent. (Other investigators (12, 39) have found it necessary to insert a voltage compensator between the reference electrode and point *B* because of the substantially lower values of shunting resistances.) Channel 1 monitored the potential difference between points *A* and *C* whereas channel 2 monitored the potential difference between points *A* and *E*; *i.e.*, across the 50 MΩ resistor. Current was calculated from the voltage drop across the 50 MΩ resistor; the voltage deflection was linearly proportional to current flow (up

to the limits of the preamplifier). The current measured by this means compared closely with that calculated from the known voltage output of the stimulator and the total resistance of legs *AB* and *CD*. Because of the high resistances in leg *AD* (and in the non-cellular parts of leg *AB*) relative to the resistance of the cell, the current flow was constant for a given voltage output of the stimulator; *i.e.*, the cell membrane was "current-clamped."

The general operation of the bridge was as follows. The bridge circuit was balanced prior to the microelectrode impalement. Balance was achieved when the ratios of resistances were equal: $R_{CD}/R_{BC} = R_{AD}/R_{AB}$. The microelectrode resistance did not substantially alter during passage of current less than 3×10^{-9} amp. At balance, there is no potential difference between points *A* and *C* due to the current flow; the same analysis holds when points *A* and *C* are at a sustained potential difference (resting potential). Following impalement of a cell, the bridge was "unbalanced" due to the resistance of the cell. The voltage drop produced by the current (change in transmembrane potential) is monitored across this cellular resistance (mainly due to the cell membrane). In some cases, the cell resistance was determined by returning the bridge to balance and calculating the total resistance in leg *AB* using the bridge ratio before and after impalement; subtraction of these two values gives the resistance of the cell. If the bridge were not exactly balanced prior to impalement, then the deflection of the potential during passage of current was not due entirely to a change in transmembrane potential of the cell but included voltage drops across non-cellular resistances as well. Therefore, after removal of the microelectrode from the cell, the same steps of current were again passed. The differences, after subtraction of these values from those obtained during impalement, are the true changes in transmembrane potential.

Time constant (T_m) and capacitance (C_m) of the cell membrane were measured using an AC bridge (*inset* of Fig. 1). Leg *AB* contains the resistance (R_{elec}) and lumped capacitance (C_{elec}) of the microelectrode as well as the resistance (R_{cell}) and capacitance (C_{cell}) of the cell; the latter are shorted when the microelectrode is not in a cell (*switch* in figure). The major resistance of the cell membrane is known to be in parallel with the membrane capacitance; the major capacitance of the microelectrode has been assumed to be in parallel with the resistance (although when in a cell there probably is a small electrode capacitance shunted between points *A* and *B*). Relatively simple solutions for the bridge unknowns were obtained by the insertion into leg *BC* of two parallel, variable resistance-capacitance networks corresponding to those in leg *AB*.

The general operation of this AC bridge was as follows. (*a*) The bridge was balanced with the microelectrode extracellular using R_E and C_E and rectangular pulses of 20 to 50 msec. duration. Balance was achieved by varying R_E until the DC component of the pulse was nulled and by varying C_E until the on-off transients were minimized. The microelectrode capacitance was of the order of 110 pf. With the microelectrode extracellular, the input capacitance to preamplifier *V* was optimally neutralized by means of the ramp method (23). (*b*) Upon satisfactory impalement of a cell (as determined by a substantial resting potential), the rectangular pulses were again applied. The time constant and the magnitude of the voltage deflections on

channel 1 were measured. The time constant of the cell (about 10 msec.) was directly measured from these data. The resistance of the cell was calculated from the magnitude of current passed through the cell. (*c*) R_C was varied until the DC component of the rectangular pulse was nulled and then C_C was varied until the on-off transients were minimized. Thus, with such an AC bridge, independent measurements of the resistance, capacitance, and time constant of a cell can be obtained.

RESULTS

I. *Effect of Current upon Frequency of Discharge*

A. DRIVEN CELLS (NON-PACEMAKER, LATENT PACEMAKER)

Many of the impaled cells were driven; *i.e.*, they did not fire due to their own pacemaker potentials but rather due to interaction with neighboring cells. The driven cells included non-pacemaker and latent pacemaker cells. The non-pacemaker cells within this group showed no evidence of pacemaker potentials; the latent pacemaker cells possessed pacemaker potentials but were driven at faster rates by neighboring cells. The frequency of discharge in driven cells was generally higher than that in non-driven cells. For example, frequencies above 60 impulses/min. were never seen in true pacemaker cells which fired due to their own pacemaker potentials, whereas frequencies up to 130 impulses/min. were observed in driven cells. It seems likely that such high driving frequencies are obtained by action of two or more pacemaker cells upon the impaled cell. Pacemaker cells were not morphologically distinct from non-pacemaker cells; furthermore, in a few cases it appeared that non-pacemaker cells became transformed into pacemaker cells and *vice versa*. In addition, 60 to 70 per cent of all impaled cells were categorized as pacemaker cells (including true, latent, and dormant pacemakers).

Our criterion for identification of a driven cell (in addition to lack of pacemaker potential in the non-pacemaker cell) was the lack of effect of depolarizing and hyperpolarizing current on the frequency of discharge. Fig. 2 illustrates one such cell and the experimental points from this cell are plotted in Fig. 5 as inverted open triangles. In Fig. 2 A–G, progressive increments of depolarizing current were applied; the frequency of discharge was not affected even though the spike magnitude was drastically diminished. The magnitude and time of application of the current in this and all succeeding figures are indicated by the current trace (see figure legends). The bridge was slightly unbalanced in F–G due to increased electrode resistance with higher currents. In H–O, progressive increments of hyperpolarizing current were applied; again the frequency was not affected even though the spike magnitude was greatly enhanced. The driving prepotentials were included in the frequency determinations regardless of the spike failures; justification for this is self-evident from Fig. 2. For example, the current intensity in O is

the same as that in P, yet in the former only prepotentials were observed. Hence the prepotentials indicate a driving rate equal to the discharge rate when the excitability of the cell is sufficiently high naturally (F) or artificially with depolarizing current (G). In Fig. 5 are plotted the data of five non-pacemaker cells, including the cell illustrated in Fig. 2. These plots show that non-pacemaker cells are insensitive to depolarizing or hyperpolarizing current.

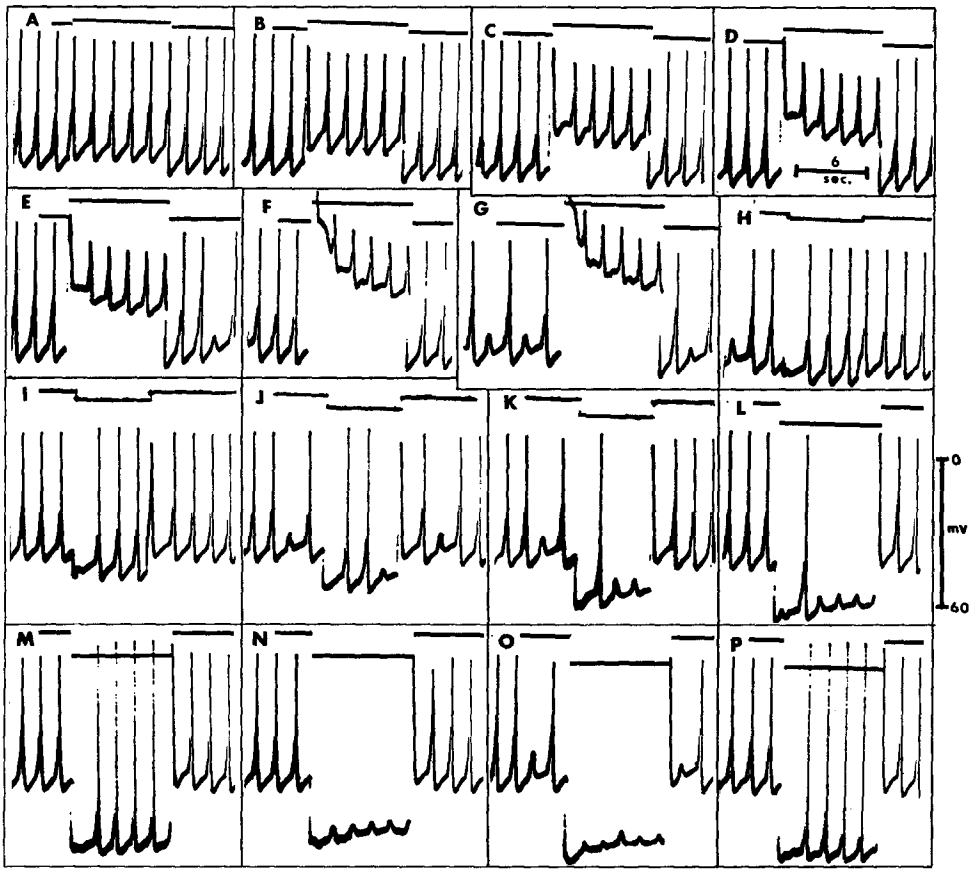

FIGURE 2. Lack of effect of current on frequency of discharge of a driven cell. *Upper traces* are current intensities and *lower traces*, transmembrane potentials; upward deflections of current traces mark application of depolarizing current and downward deflections, hyperpolarizing current. Vertical voltage calibration, in L represents 60 mv and horizontal time calibration in D, 6 sec. Bridge in good balance in all photos except F–G. A–G, progressively increasing depolarizing current steps; note the progressive diminution in spike height but the unchanged frequency of firing. In E and G some of the spikes failed to be triggered by the "prepotentials;" such failures have been included for purposes of frequency determinations. H–O, progressively increasing hyperpolarizing current steps; note progressive enhancement of spike height but unchanged frequency of firing. P, same current step as in O. Note positive after-potentials and off-excitation following hyperpolarizing pulses.

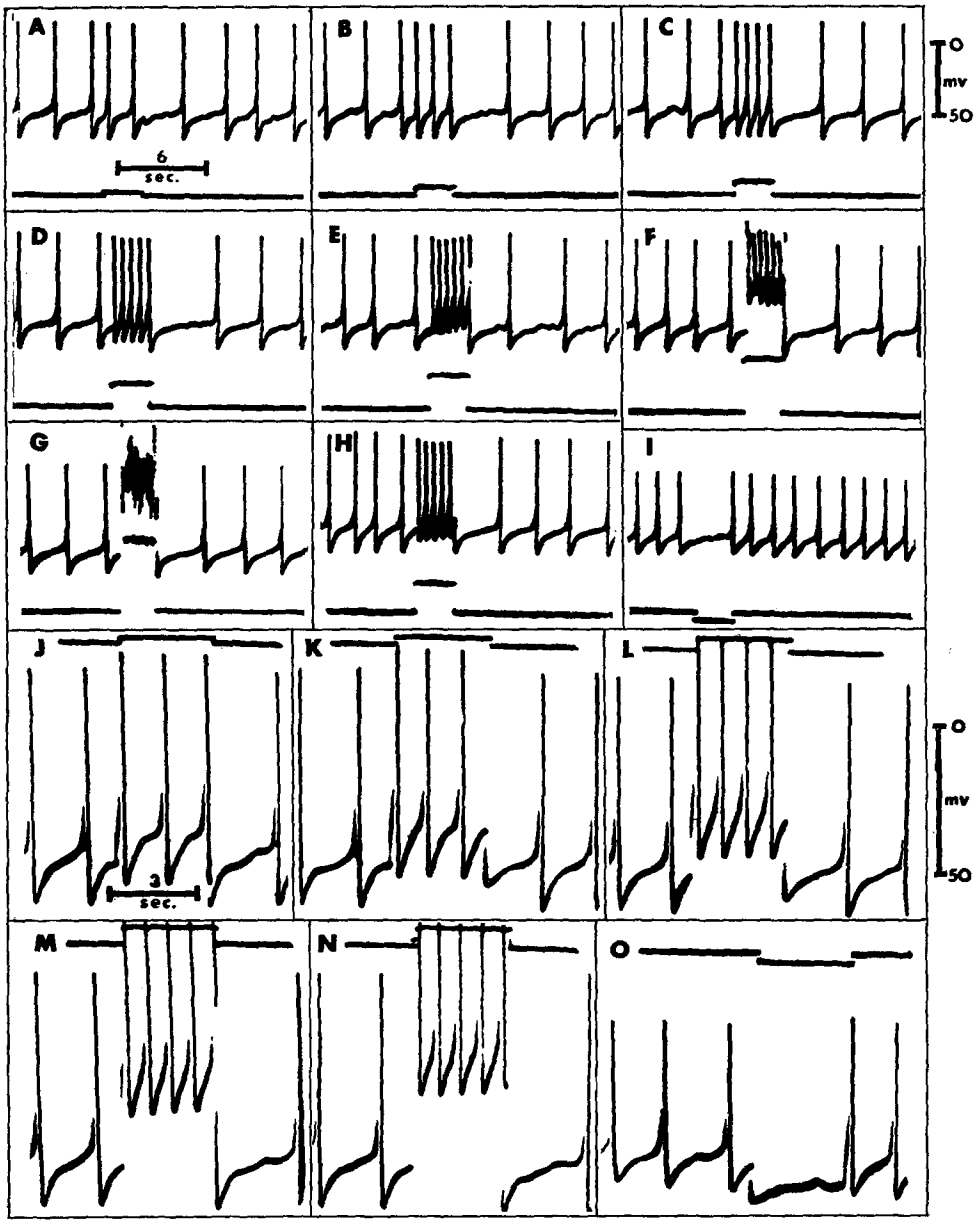

FIGURE 3. Effect of current on the frequency of discharge of pacemaker cells. In all photos, upward deflections of current traces mark application of depolarizing current and downward deflections, hyperpolarizing current. A–I, one cell. *Upper traces* are transmembrane potentials and *lower traces*, current intensities. Voltage calibration in C represents 50 mv and time calibration in A, 6 sec. Progressively increasing depolarizing current steps shown in A–G; note the increased frequency of discharge. Diminution of current intensity in H results in a lowered frequency of discharge. A hyperpolarizing current pulse is shown in I; note that the discharge was abolished and the slope of the pacemaker potential diminished. Bridge balance good in all photos, except F–G. J–O, second cell. *Upper traces* are current intensities and *lower traces*, transmembrane potentials. Voltage calibration in L represents 50 mv and time calibration in J, 3 sec. Progressively increasing depolarizing current steps are shown in J–N and a hyperpolarizing current pulse in O. Peaks of the action potentials obscured in N due to bridge imbalance. In both cells, note the pronounced positive off-potentials produced immediately following cessation of the depolarizing current pulses and off-excitation following hyperpolarizing pulses.

B. NON-DRIVEN CELLS (TRUE PACEMAKER, DORMANT PACEMAKER)

Many of the cultured ventricular cells were non-driven and possessed pacemaker potentials which averaged about 10 mv with slopes of about 10 mv/sec. (22); these were considered true pacemaker cells. The effect of current upon the frequency of discharge was determined; Fig. 3 shows two such cells (A–I and J–O). In A–G, progressive increments of depolarizing current were applied followed by a return to a lower current intensity in H; similar increments were applied in J–N. The frequency of discharge was increased as a function of the intensity of current and rapidly returned to about the basal rate following cessation of current. Hyperpolarizing current of low intensity slowed the frequency, and current of high intensity abolished the discharge as shown in I and O. The bridge became unbalanced in G due to an increase in microelectrode resistance during passage of highest current (about 4×10^{-9} amp) and in J–O perhaps due to pressure upon the electrode during impalement. The experimental points from these two cells are plotted in Fig. 5 as closed circles (A–I) and open circles (J–O); in addition, the data from two other such cells are plotted. The relationship between frequency of pacemaker cell discharge and polarizing current appears to be sigmoid with a linear, steep portion between 0 and 1.2 nanoamperes of depolarizing current; the slope of this linear region is about 58 impulses/min. per 1.0 nanoampere.

Some of the cells did not fire action potentials and had a fairly stable resting potential; *i.e.*, little or no pacemaker potential. However, during passage of depolarizing current, such cells often fired repetitively and pacemaker potentials became clearly evident. For these reasons, such cells may be considered dormant pacemakers. Fig. 4 illustrates three such dormant pacemaker cells (A–H, I–M, and N–S). In A–G, I–M, and N–Q progressive increments of depolarizing current were applied. The frequency of discharge initiated by the current was a function of the current intensity; the latent period between application of current and the first response also was a function of current intensity (A and D or J and L). Following cessation of current the frequency of discharge immediately returned to zero. Excessive depolarization abolished the action potentials and gave rise to oscillations in membrane potential; this is evident in G, P, and Q, although high frequency, low voltage oscillations in Q are not resolvable in the figure. The four steps of current in N–Q are shown superimposed as four successive sweeps in R and the bridge imbalance to these same four steps of current is shown superimposed in S. At low values of resting potential similar small, high frequency oscillations in membrane potential were observed which were graded with the intensity of hyperpolarizing current; similar graded oscillations have been reported for smooth muscle (27). Sometimes a dormant pacemaker cell fired an occasional

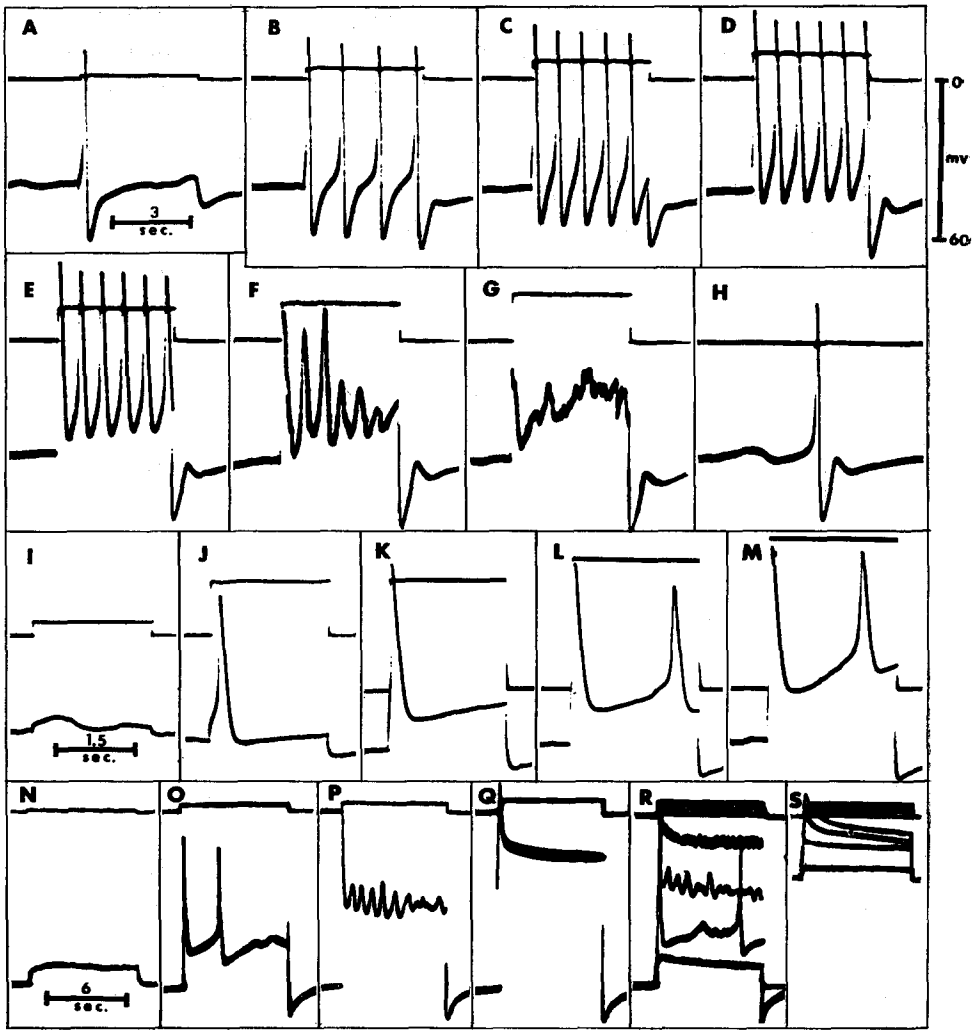

FIGURE 4. Effect of current on the frequency of discharge of dormant pacemaker cells. *Upper traces* are current intensities and *lower traces*, transmembrane potentials; upward deflections of current traces mark application of depolarizing current. Voltage calibration in D represents 60 mv and time calibration in A, 3 sec. (A–H), 1.5 sec. (I–M), and 6 sec. (N–S). A–H, one cell. Progressively increasing depolarizing current steps in A–G; note discharges initiated in the quiescent cell and increase in slope of the pacemaker potentials. In G, action potentials failed due to excessive depolarization and irregular oscillations were produced. In H is shown an action potential from the same cell spontaneously occurring later in time. I–M, second cell showing progressively increasing steps of depolarizing current; note the concomitant increase in slope of the pacemaker potential. N–S, third cell showing four progressively increasing depolarizing current steps in N–Q; these same four steps are superimposed in R and the corresponding blank bridge imbalances are shown in S. Note that oscillations are produced with the two largest current steps (P–R); the high frequency, low voltage oscillations in Q–R are not resolvable in the photo. In all three cells, note the pronounced positive off-potentials produced immediately following the cessation of the current pulses.

action potential; one such spontaneous action potential is shown in H for purposes of comparison with the evoked responses. Hyperpolarizing currents were generally without effect although occasionally "off-excitation" occurred; *i.e.*, a response upon the cessation of the hyperpolarization. The experimental points from two of these cells are plotted in Fig. 5 as closed triangles (A–H) and open triangles (N–S).

The other category of pacemaker cells, called latent pacemakers, exhibit

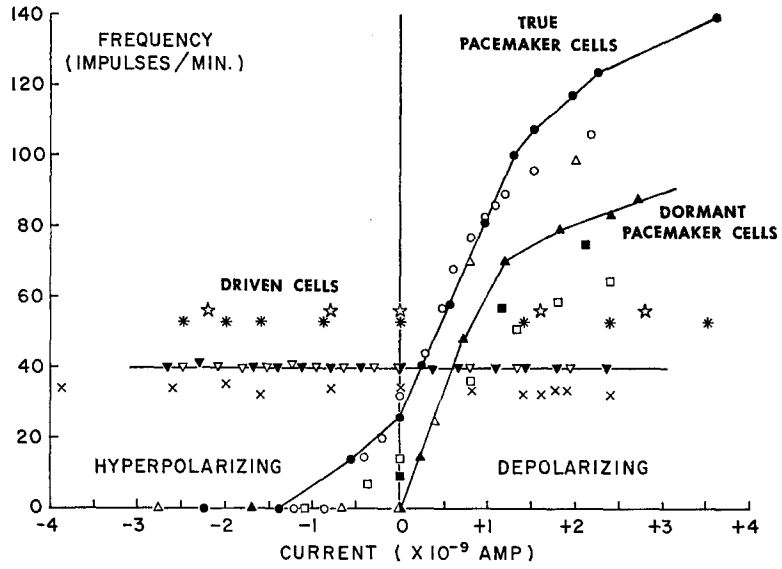

FIGURE 5. Effect of depolarizing and hyperpolarizing current upon the frequency of discharge of true pacemaker, dormant pacemaker, and driven cells. Constant current pulses applied by means of a bridge circuit so that one microelectrode could be used for recording transmembrane potentials and simultaneously passing current. Note the sensitivity and lack of sensitivity to current in the two types of cells. Individual symbols represent multiple measurements at different current levels in the same cell. Curves drawn through data obtained from one cell of each of the three types, true pacemaker, dormant pacemaker (zero spontaneous frequency), and driven cells (including non-pacemakers and latent pacemakers).

pacemaker potentials but are driven at a faster rate *via* transmission of excitation from other cells. There is usually a prepotential superimposed upon the pacemaker potential; this prepotential and not the pacemaker potential actually triggers the spike (22). In such cells, depolarizing current does not necessarily alter the rate of firing provided the driving prepotentials occur at a fast rate.

The effect of current upon the discharge frequency in pacemaker cells appears to be mediated mainly *via* a change in slope of the pacemaker potential ($\dot{V}_p$). Figs. 3 and 4 show very clearly that such is the case. In particular, in Fig. 3 A–D, J–L, and Fig. 4 A–D, I–M, N–O, progressive incre-

ments of depolarizing current led to marked increases in the slope of the pacemaker potential. The pacemaker potential is recognized as a prominent change in slope of the membrane potential following the positive after-potential. In Fig. 3 I, O hyperpolarizing current led to decreased $\dot{V}_p$ with concomitant decrease in frequency of discharge. The experimental points obtained from Figs. 3 and 4 are plotted in Fig. 6 as closed circles (Fig. 3 A–I), closed triangles (Fig. 3 J–O), open circles (Fig. 4 A–H), and closed squares (Fig. 4 I–M). With zero current, $\dot{V}_p$ varied between 3 and 15 mv/sec.

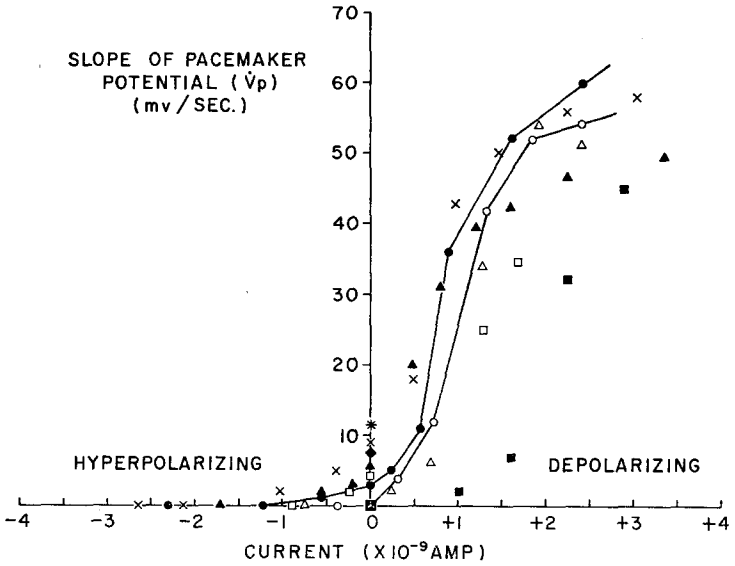

FIGURE 6. Effect of depolarizing and hyperpolarizing current upon the slope of the pacemaker potential ($\dot{V}_p$); current applied through a bridge circuit. With zero current, $\dot{V}_p$ in most pacemaker cells varied between 3 and 15 mv/sec. Individual symbols represent multiple measurements in the same cell; curves drawn through data obtained from one true pacemaker cell and one dormant pacemaker cell.

in most pacemaker cells. In Fig. 6, the data from seven cells show the effect of depolarizing and hyperpolarizing current on $\dot{V}_p$; curves are drawn through one pacemaker cell and through one dormant pacemaker cell. The general shape of these curves is sigmoid with the steepest, rather linear portion between about 0.6 and 1.2 nanoamperes of depolarizing current. The data from five cells of Figs. 5 and 6 are replotted in Fig. 7 in which the frequency is expressed as a function of $\dot{V}_p$. The solid curve is drawn through the experimental points obtained from one cell. This curve is steep between values for $\dot{V}_p$ of 0 to 10 mv/sec. and then gradually flattens. If the experimental points are replotted semilogarithmically, frequency becomes a linear function of the logarithm of $\dot{V}_p$ between 1 and 30 mv/sec. with a change of about 46

impulses/min. per tenfold change in $\dot{V}_p$; this curve had a steeper slope above 30 mv/sec. The dotted line in Fig. 7 was calculated assuming: (*a*) the critical depolarization necessary to reach threshold to be 10 mv (*i.e.*, a V_p of 10 mv), (*b*) a total "refractory" period of 0.4 sec. in each cycle consisting of the action potential and positive after-potential during which V_p is reset to zero, and (*c*) the length of the refractory period is unchanged at different frequencies. The dashed line represents the linear relationship between frequency and $\dot{V}_p$ previously reported for cultured chick heart cells (8).

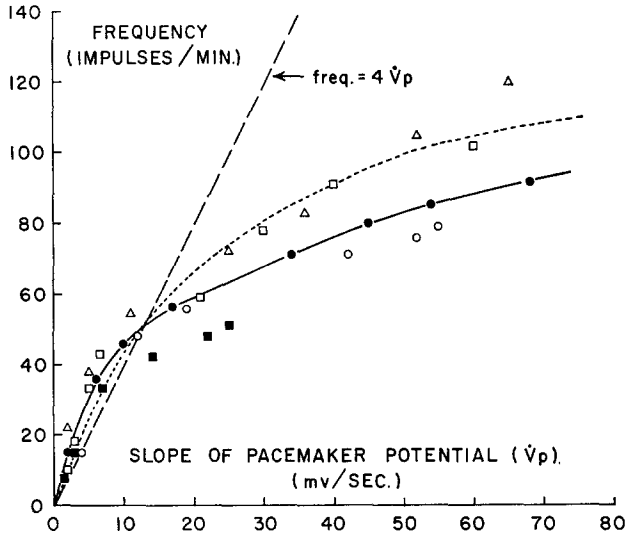

FIGURE 7. Relationship between frequency of discharge and slope of the pacemaker potential ($\dot{V}_p$). Data replotted from Figs. 5 and 6, except where it was not possible to measure $\dot{V}_p$ with any accuracy. Individual symbols represent multiple measurements in the same cell; curve drawn through data obtained from one cell. Dotted line was calculated (see text). Dashed line represents the linear relationship between frequency and $\dot{V}_p$ reported for cultured chick heart cells (8).

II. *Effect of Current upon the Magnitude of Responses*

A. ACTION POTENTIALS

Current flow had a pronounced effect on the magnitude of the action potential in both pacemaker and non-pacemaker cells. Depolarizing current diminished and hyperpolarizing current enhanced the action potentials as is evident in Figs. 2 A–P, 3 A–F, 10 C–E, J–L, and 11 H–I. Observations made on twelve cells are plotted in Fig. 8 and a curve has been drawn for the data from one cell. The relationship between relative spike magnitude and current is linear between ±4 nanoamperes of current; the curve passes through the origin. The slope ranged between 11 to 42 per cent change in spike height per 1.0 nanoampere. The slope of the curve in Fig. 8 is 22 per

cent/nanoampere; the slope depends upon the cell resistance. Thus, for a mean action potential of 72 mv, the spike height would be changed about 16 mv per nanoampere (or per 12 mv change in resting potential for a mean cell resistance of 12 MΩ).

B. POSITIVE "OFF-POTENTIAL" ON CESSATION OF CURRENT

A pronounced positive off-potential was produced upon the cessation of a depolarizing current pulse in all pacemaker and in some driven cells; the only requirement seemed to be that the cells have a natural positive after-

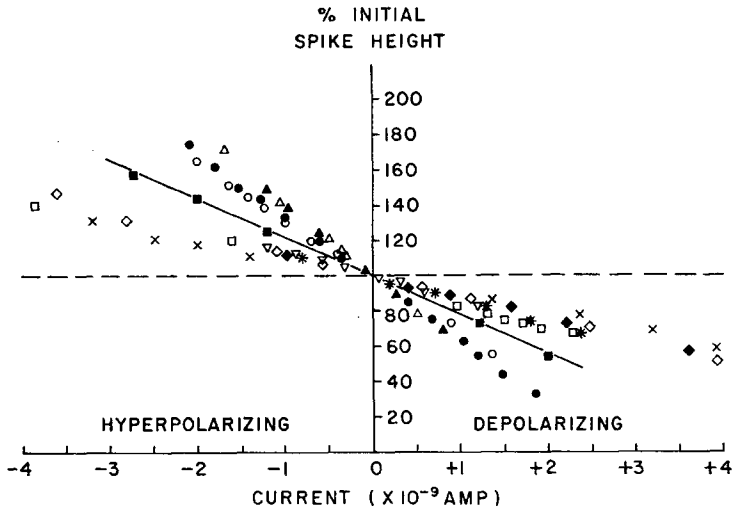

FIGURE 8. Effect of depolarizing and hyperpolarizing current upon the relative magnitude of the action potentials; current applied through a bridge circuit. In pacemaker and non-pacemaker cells, the spike height decreased with depolarization and increased with hyperpolarization. Individual symbols represent multiple measurements at different current intensities in the same cell; curve drawn through data obtained from one cell.

potential. This phenomenon is shown most clearly in Fig. 3 D–G, K–N, and Fig. 4 A–G, I–M, N–R; the magnitude of the off-potential was a function of the intensity of the depolarizing current. The phenomenon occurred even under conditions in which no action potentials were triggered during the depolarizing pulse (Figs. 3 G, 4 G, I, N, P–Q). Similar positive off-potentials were produced in cells impaled by microelectrodes filled with 3 M NaCl. The observations obtained from eight cells which did and from two cells which did not exhibit the phenomenon are plotted in Fig. 9; a curve has been drawn through the data obtained from one cell. This curve has the steepest slope between about 0.1 and 0.6 nanoampere of depolarizing current; a replot of the experimental points semilogarithmically indicated a linear relationship

between 0.1 and 3 nanoamperes with a slope of about 15 mv change in off-potential per tenfold change in current intensity. As shown in Fig. 9, off-potentials as large as 26 mv were obtained. In addition, in a given cell at a constant current intensity, the magnitude increased, within limits, with duration of application of the pulse. A second (delayed) small positive off-potential was occasionally seen following the initial large positive off-potential produced by strong depolarizing currents (Fig. 4 D–G). It is interesting to

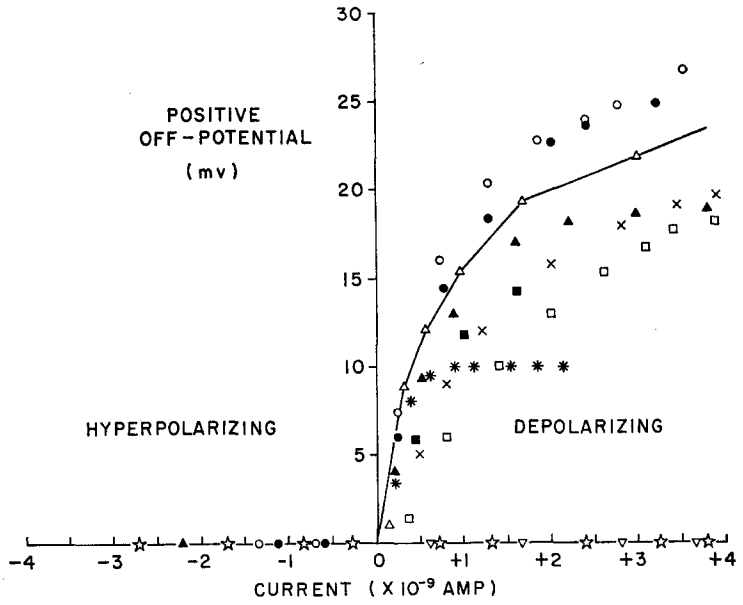

FIGURE 9. Effect of polarizing current upon the magnitude of the positive off-potential produced upon the cessation of a depolarizing pulse in pacemaker and dormant pacemaker cells and other cells which showed regular positive after-potentials. Individual symbols represent multiple measurements in the same cell; curve drawn through points obtained from one cell. Similar positive off-potentials were produced using microelectrodes filled with 3 M NaCl.

note that following a spontaneous action potential, there occurs a similar second (delayed) positive after-potential (Fig. 4 H). As shown in Fig. 9, hyperpolarizing current did not elicit the positive off-potential. However, hyperpolarizing current of "threshold" intensity or above, did lead to the phenomenon of off-excitation, *i.e.*, an action potential was initiated at the cessation of the hyperpolarizing pulse. This is evident in Figs. 2 I–P, 3 O, and 11 C–F.

C. PREPOTENTIALS

Prepotentials have been found previously in cultured chick embryonic cardiac cells (22). In the present study, the effect of current upon the magni-

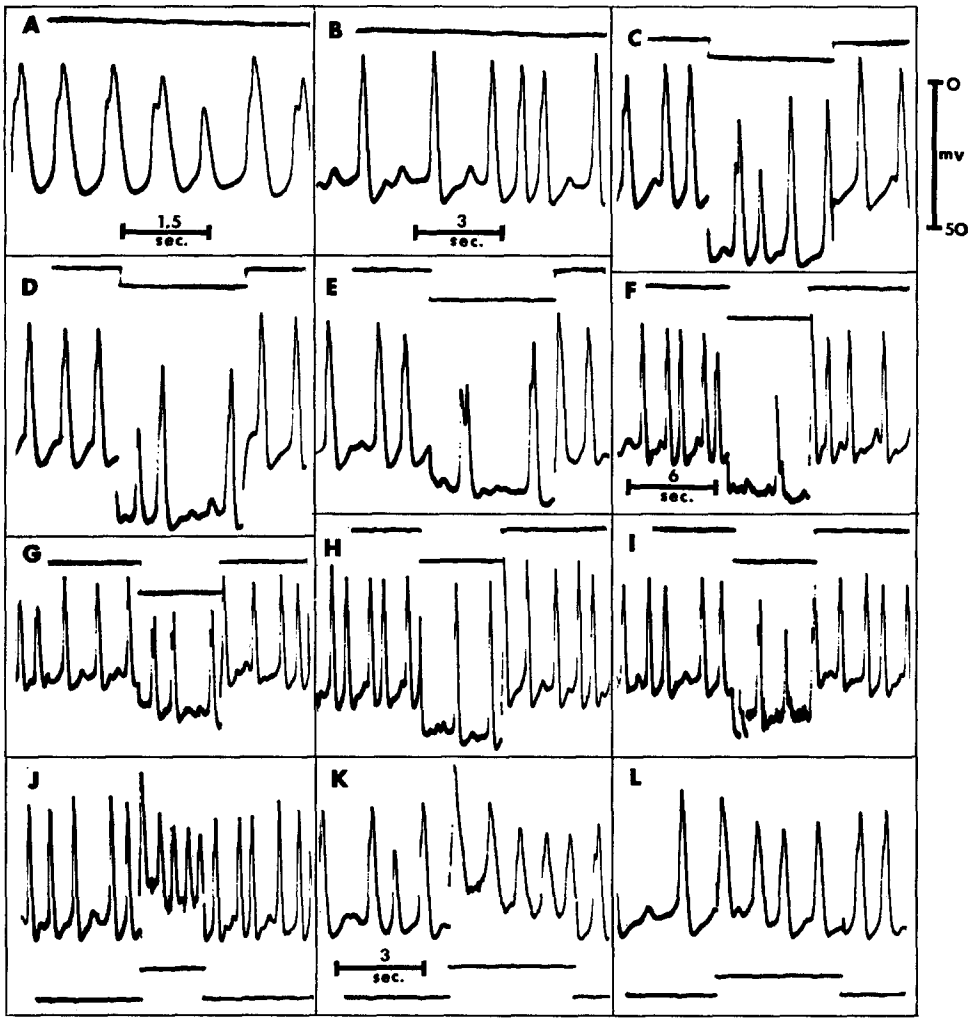

FIGURE 10. Effect of current on large prepotentials in a driven cell. Voltage calibration in C represents 50 mv in all photos and time calibrations in A represent 1.5 sec. (A), in B, 3 sec. (B–E), in F, 6 sec. (F–J), and in K, 3 sec. (K–L). The current channel is the *upper trace* of A–I and the *lower trace* of J–L. A–B, current not applied; shows natural occurrence of large and small prepotentials. The large prepotentials may occur on the rising phase of the spike or may occur without spike responses; in the latter case, note the smaller total duration of each response. C–I, various steps of hyperpolarizing current applied which, in all instances, led to enhanced magnitudes of the large type of prepotential but had relatively little effect upon the small prepotentials. Enhancement of the large prepotential is produced even when it occurs without a spike as a result of the hyperpolarization (C–F, I). Note in G that the spike is initiated later on the falling phase of the prepotential. J–L, various steps of depolarizing current applied which, in all instances, led to diminished large prepotentials on the rising phase of the action potentials and led to more successful transmission as evidenced by the increased frequency of action potentials.

tude of the prepotentials was determined. The prepotentials can be arbitrarily classified into small and large types. Either type could occur isolated or as a prominent step on the rising phase of the action potential. Prepotentials were generally found only in driven cells (non-pacemakers and latent pacemakers); *i.e.*, cells in which polarizing currents had no effect on the frequency of the action potentials or prepotentials. Some cells exhibited large and small prepotentials (Fig. 10). The small prepotential is illustrated in Figs. 2 E–O, 10 B–L, and 11 A–G, and the large prepotential, in Fig. 10 A–L. Neither depolarizing nor hyperpolarizing current appeared to affect the magnitude of the small prepotentials (Figs. 2, 10, 11); see Fig. 10 F for a possible exception. However, hyperpolarizing currents increased and depolarizing currents decreased the magnitude of the large prepotential (Fig. 10); these changes in relative prepotential height with current roughly paralleled the curve for spike height shown in Fig. 8. That is, the spike and the large prepotential were affected by polarizing currents to about the same degree. Depolarizing currents led to more successful transmission, as evidenced by the increased frequency of action potentials (Fig. 10 J–L). The durations of the prepotentials are not greatly different than are those of the spikes (Fig. 10 A, C–D). The prepotentials appear to have exponential decays and the rising phases are substantially faster than the decays (Figs. 10 C–D and 11 A, F). Both types of prepotential may represent synaptic interaction between adjacent cardiac cells and the difference in their magnitudes may be a function of the distance between the synaptic junctions and the microelectrode (see Discussion).

In Fig. 11 A–G, the small prepotentials spontaneously vary in magnitude up to a threshold firing level. Close examination reveals a decrease in slope on the rising phase of these enhanced prepotentials which occurs at about a constant level of membrane potential (Fig. 11 A–C); hyperpolarizing current abolished the spontaneous enhancement of the small prepotential. It is probable that the second component of the enhanced prepotentials represents the "local excitatory response;" *i.e.*, an active response of the membrane due to the driving prepotential. It should be noted that the frequency of response in the cell represented by Fig. 11 A–I was not affected by polarizing currents; the small, gradual diastolic depolarization evident (*e.g.*, in B) may represent a prolonged positive after-potential or a pacemaker potential of small slope. The local excitatory response became progressively larger with time following each of these gradual depolarizations.

In some experiments (Fig. 11 A–I), contractions of the impaled cell and of its neighbors were visually observed at × 600, and correlation was made with the electrical activity of the impaled cell. In all instances, a spike was accompanied by a contraction of the impaled cell (as well as the neighboring cells) whereas the local prepotential was not accompanied by a contraction

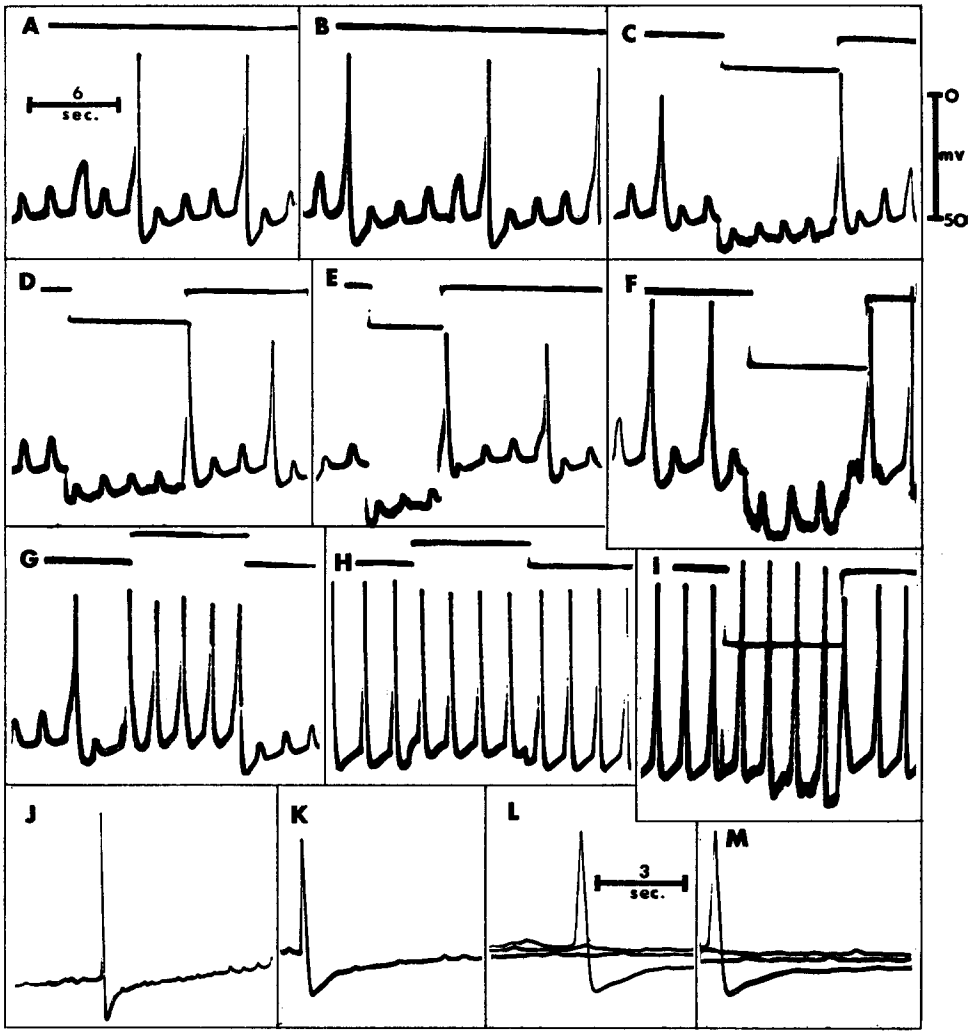

FIGURE 11. Lack of effect of current on frequency of discharge of a cell driven under conditions of partial transmission block (A–I). Voltage calibration in C represents 50 mv and time calibrations in A, 6 sec. (A–K) and in L, 3 sec. (L–M). *Upper traces* in A–I are current intensities and *lower traces*, transmembrane potentials; upward deflections of current traces mark the application of depolarizing current and downward deflections, hyperpolarizing current. Current was not applied in A–B and J–M. A–I, contractions of the impaled cell and of its neighbors were correlated with electrical activity. A spike was accompanied by a contraction of the impaled cell (as well as the neighboring cells) whereas the prepotential was not accompanied by a contraction of the impaled cell but only of the neighboring cells. In many cases transmission of excitation failed. A–B, prepotentials which occasionally successfully trigger spikes; note the variable magnitudes of the prepotentials, the slight depolarization between spikes, and the change in slope of the rising phase of the larger prepotentials. C–F, several steps of hyperpolarizing current; note enhancement of prepotentials is abolished. G, depolarizing current pulse resulted in spike triggered by each junctional potential; *i.e.*, successful transmission. H–I, same cell later attained completely successful transmission; depolarizing current (H) and hyperpolarizing current (I) affected spike height but did not change frequency of firing. J–M, two pacemaker cells (J and K–M) showing "miniature" potentials superimposed upon the pacemaker potential; note the increase in frequency and magnitude of the miniature potentials with depolarization (several sweeps superimposed in L–M).

of the impaled cell but only of the neighboring cells. Thus, the prepotential represents the transmission of excitation from adjoining cells; in many cases transmission of excitation failed (partial block). Such failures are increased under conditions of depressed excitability produced by hyperpolarizing current (Fig. 11 C–F) and decreased with enhanced excitability produced by depolarizing current (Fig. 11 G). The cell later spontaneously attained completely successful transmission (Fig. 11 H–I); depolarizing current (H) and hyperpolarizing current (I) affected the spike height but did not change the frequency of firing.

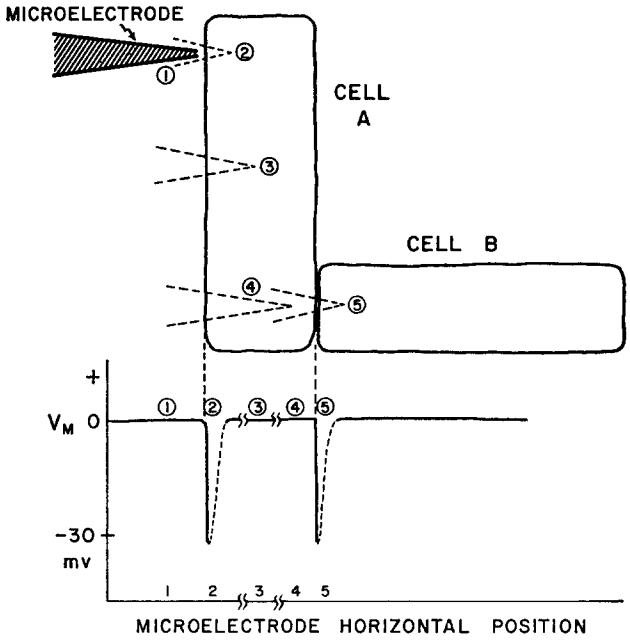

FIGURE 12. Schematic diagram of the potential profile of the junction between two isolated cultured heart cells. If cell A is depolarized and stops beating due to injury during impalement, cell B continues to beat and also shows a resting potential upon penetration of the microelectrode across the junction; *i.e.*, there is a sharp discontinuity of potential between the myoplasm of cells A and B.

Many cells, both pacemaker and non-pacemaker, were found to exhibit miniature potentials which were smaller than the small prepotentials; their magnitudes varied between 0.5 and 4 mv and they had durations of 100 to 300 msec. In many cells these miniature potentials occurred randomly during electrical diastole but in some pacemaker cells (Fig. 11 J–M) they appeared to be a function of the membrane potential. In these photos, the miniature potentials are superimposed upon the pacemaker potential; note the increase in magnitude and frequency of the miniature potentials with depolarization

(several sweeps superimposed in L–M). The relationship of these miniature potentials to the prepotentials described above is not known.

III. *Myo-Myo Junctions*

A. ARTIFICIAL EPHAPSES

Cultured cells physically separated from each other beat independently; whenever the cells grew together naturally, they usually beat synchronously

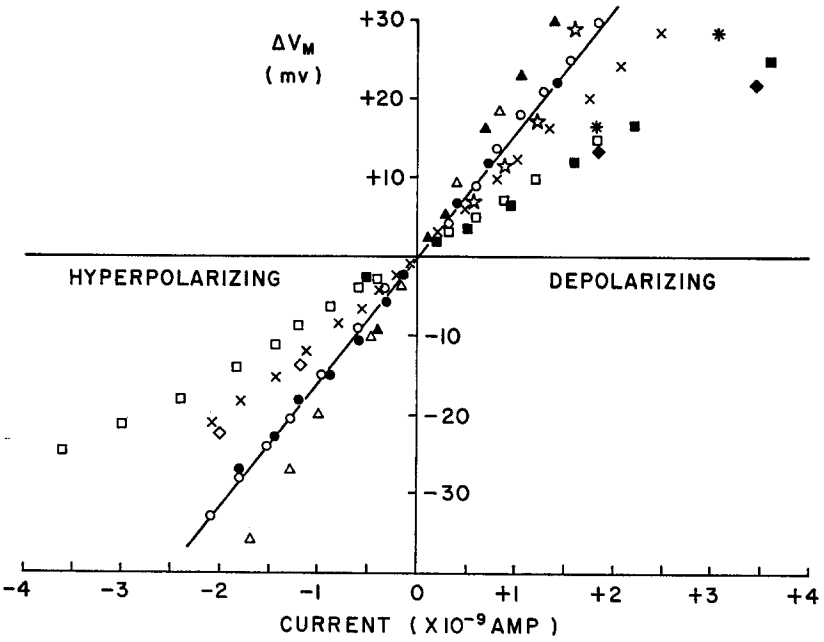

FIGURE 13. Effect of depolarizing and hyperpolarizing current upon the resting mem brane potential (V_m); current applied through a bridge circuit. The voltage/curren curves were linear for most cells between 30 mv hyperpolarization and 30 mv depolari zation and passed through the origin; the slopes varied between 7 and 20 MΩ, with a mean of 13 ± 1.2 MΩ. Individual symbols represent multiple measurements in the same cell; curve drawn through data obtained from one cell has a slope of 15 MΩ. The data have not been corrected for the slightly underestimated changes in potential (about 9 per cent),

(22). In twelve separate experiments, when two such independently beating cells were pushed together under direct visual observation they did not synchronize even though large areas were in contact for several minutes. Motion pictures of these experiments were taken for careful analysis. The cells were not injured in these experiments because they continued to beat, although independently, after being pushed into contact. Thus, such artificial ephapses do not result in significant electrotonic interaction.

B. TRANSMEMBRANE POTENTIALS AT JUNCTIONS

Two cultured cells, joined and beating synchronously, were located in fifteen separate experiments (Fig. 12). Relatively large tipped microelectrodes (1 to 3 μ) were used in order to injure and depolarize the impaled cells. Thus, it was possible to obtain the potential profile across the functional junction between the two cells. For example, as shown in Fig. 12, if cell A was impaled first in region 2, a resting potential of about 30 mv was obtained which held for a few seconds and then slowly declined to zero (indicated by dotted lines); concomitant with this depolarization, cell A stopped beating but cell B continued to beat. Now if the microelectrode was withdrawn and inserted into regions 3 and 4 in succession, still no resting potential was obtained from cell A. However, if the microelectrode were advanced into region 5 by passing across the cell junction, a sharp drop in potential again occurred. This indicated that cell B possessed a substantial resting potential at a time when its adjoining neighbor was entirely depolarized. The resting potential of cell B also gradually declined to zero with a concomitant cessation of beating. Thus, there is a sharp discontinuity of potential between the myoplasm of two adjoining cells across a functional junction; *i.e.*, there is a transmembrane resting potential across each junctional membrane.

IV. *Effect of Current upon the Transmembrane Resting Potential*

A. VOLTAGE/CURRENT CURVES (ΔVm/I)

Frequency of discharge, $\dot{V}_p$, spike height, and positive off-potential must be affected by means of changes in membrane potential (ΔV_m) produced by small polarizing currents (1 to 3 nanoamperes). Hence, the resistance of one cultured heart cell must be high in order to produce a sufficient ΔV_m. For example, a cell having a spike of 72 mv would average about a 16 mv change in spike height per 1.0×10^{-9} amp of current (Fig. 8); in order for this to be possible the cell resistance must be about 12 to 16 MΩ. In addition, the linearity of the spike height/current curve suggests that the steady-state resistance of the cell is independent of V_m (*i.e.*, there is no rectification) with hyperpolarizations and depolarizations of 28 to 42 mv.

However, separate voltage/current curves were obtained in which the effect of current upon the transmembrane resting potential was measured directly. Fig. 13 shows the observations obtained from ten cells; a curve is drawn through the values obtained from one cell. The curves were linear for most cells between hyperpolarizations and depolarizations of 30 mv and passed through the origin. The slopes varied between 7 and 20 MΩ, with a mean value of 13 $\pm$ 1.2 MΩ. Thus, in the majority of cells there was no evidence of rectification within these limits of changes in transmembrane

potential. The data agree closely with the cell resistance value and lack of rectification predicted by Fig. 8.

B. MEASUREMENT OF R_{cell}, C_{cell}, AND T_m

The cell resistance (R_{cell}), the cell capacitance (C_{cell}), and the membrane time constant (T_m) were measured directly and simultaneously by varying the bridge parameters. (*a*) With the DC bridge, R_{cell} was determined by

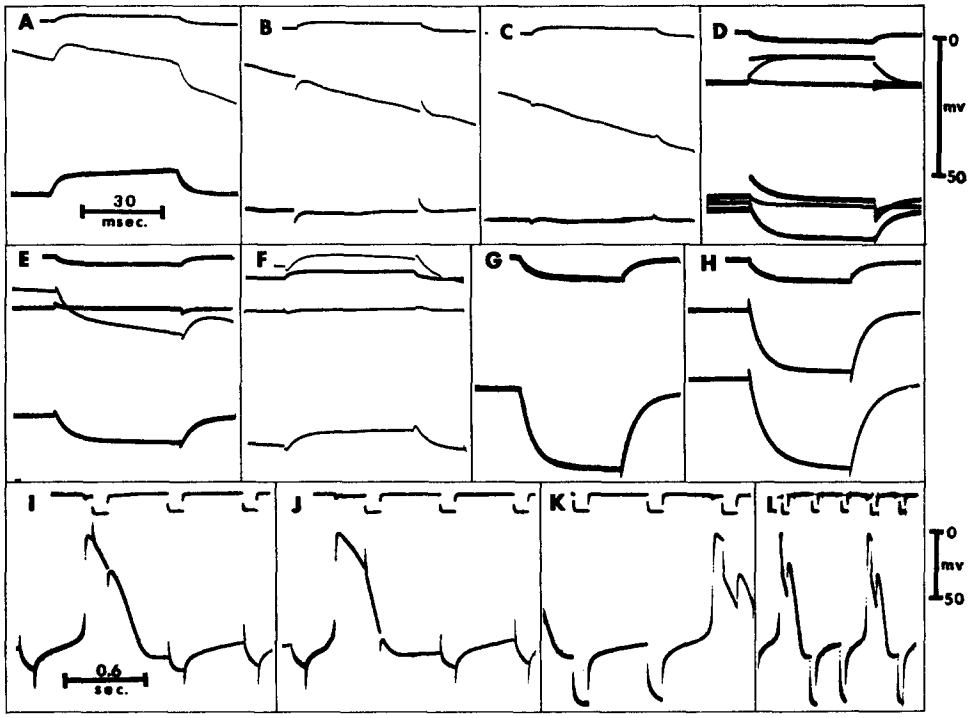

FIGURE 14. Resistance, capacitance, and time constant measurements during resting potential (A–H) and pacemaker potentials (I–L). The voltage calibration in D represents 50 mv in A–F and that in L represents 50 mv in G–L. Time calibration in A represents 30 msec. in A–H, that in I represents 0.6 sec. in I–K, and 1.5 sec. in L. In all photos, current channel is *upper* trace and *lower channel*, transmembrane potential. Depolarizing current applied in A–C and F, hyperpolarizing current in D–E, G–L; greater current intensity applied in G–L. DC bridge (G–L) and AC bridge (A–F). Two successive sweeps superimposed in A–C, E–F, H show the application of the pulse also during the action potential (uppermost trace in F). Extra trace in E–F represents the blank with microelectrode extracellular. A–C, sequence from same cell while varying the bridge parameters. In D, six successive sweeps are superimposed, three with the microelectrode intracellular and three, extracellular; AC bridge parameters varied for balance. See text for further explanation. I–L, application of constant current pulses *via* DC bridge showing increase in magnitude and time constant of transmembrane potential change in later regions compared to that in earlier regions of the pacemaker potential in two cells (I–J and K–L); bridge unbalanced in K–L.

adjusting the resistance of leg *CD* until the voltage deflections were again nulled. The total resistance in leg *AB* was calculated using the bridge ratio before (R_{elec}) and after ($R_{elec} + R_{cell}$) impalement; subtraction of these two values gives R_{cell}. By this method, a mean value of 12 ± 1.5 MΩ was obtained for R_{cell} in a total of twenty-two measurements. (*b*) With the DC bridge, R_{cell} was also determined by nulling the bridge prior to impalement (balance out R_{elec}) and measuring the DC voltage deflections to the applied current pulses following impalement (Figs. 13 and 14 G–H). R_{cell} was calculated by

TABLE I

SUMMARY OF MEASUREMENTS OF RESISTANCE, CAPACITANCE, AND TIME CONSTANT USING THE AC BRIDGE METHOD*

	Bridge				Calculated			Measured
Current	R_E	C_E	R_C	C_C	R_{cell}	C_{cell}	T_m	T_m
nanoamperes	*KΩ*	*μf*	*KΩ*	*μf*	*MΩ*	*pf*	*msec.*	*msec.*
−0.51	48	0.065	13	0.48	7.2	873	6.3	8.0
	50	0.062	16	0.55	8.8	1000	8.8	9.8
	94	0.050	17	0.30	9.3	545	5.1	6.4
	45	0.066	12	—	6.6	—	—	8.7
+0.51	141	0.033	29	0.40	16.0	727	11.6	10.0
	176	0.018	24	0.40	13.2	727	9.6	9.5
	113	0.029	25	0.45	13.8	818	11.3	9.0
	103	0.030	38	0.23	20.9	418	8.7	14.3
−1.31	128	0.027	14	0.70	7.7	1273	9.8	8.0
	110	0.032	13	0.65	7.2	1182	8.5	6.9
Mean	101	0.041	20	0.46	11.1	840	9.3	9.1
SEM	±8	±0.004	±1.6	±0.03	±0.9	±54	±0.4	±0.4
n	30	30	30	27	30	27	27	30

* Each value in the table is the mean obtained from three cells.

measurement of the voltage deflections produced by known steps of current. This is the method used for the voltage/current curves described above (Fig. 13). In addition, T_m can be estimated simultaneously by speeding up the sweep and measuring the charging time for the membrane capacitance-resistance network (Fig. 14 G–H); a mean value of 12 ± 1.6 msec. was obtained for T_m in twelve measurements. However, this method of measuring T_m is not accurate because the time constant of the microelectrode cannot be easily separated from that of the cell. (*c*) To obviate this latter difficulty and obtain a true value for T_m, an AC bridge was used in order to balance out C_{elec} as well as R_{elec} (see Methods). (*d*) By insertion of the variables R_c and C_c into leg *BC* of the AC bridge, it was possible to measure directly C_{cell}, as well as R_{cell} and T_m. Thus, it was possible to calculate as well as to meas-

ure directly T_m for comparison. C_{cell} was calculated by dividing the value of C_c at null by the bridge ratio of 550 and R_{cell} was calculated by multiplying R_c by 550. Table I is a summary of such measurements of resistance, capacitance, and time constant using this AC bridge method and Fig. 14 A–F shows some typical experiments. Depolarizing current was applied in A–C, F and hyperpolarizing current in D–E. Two successive sweeps superimposed in A–C, E–F show the application of the pulse before and during the action potential; extra trace in E–F represents the "blank" with microelectrode extracellular. A–C is a sequence from the same cell while varying the bridge parameters. In A, R_c and C_c were zero and the voltage deflection represents the voltage drop across R_{cell}; in B, R_c was varied until the DC component was nulled and in C, C_c was also varied until the on-off transients were minimized. These same three conditions are shown superimposed in D in another cell; in addition, the three upper voltage traces represent the same conditions with the microelectrode extracellular. E–F shows the condition with R_c and C_c at zero in two different cells. As shown in the table, for a total of thirty cells a mean value of 11.1 ± 0.9 MΩ was obtained for R_{cell}, 840 ± 54 pf for C_{cell}, 9.3 ± 0.4 msec. for T_m (calculated), and 9.1 ± 0.4 msec. for T_m (measured). The various methods described give values of R_{cell}, C_{cell}, and T_m in close agreement. Assuming ribbon-like cells 100 μ long, 15 μ wide, and 5 μ thick, and neglecting the longitudinal resistance of the myoplasm, the calculated specific membrane resistance (R_m) is 480 Ω-cm² and the specific capacitance (C_m), 20 μf/cm² using average values of 12 MΩ and 800 pf for R_{cell} and C_{cell}, respectively (see Table II).

C. CHANGE IN R_m WITH V_p

Brief (50 msec.) polarizing constant current pulses were applied through the DC bridge during the pacemaker potential of eight cells. The results of two such experiments using hyperpolarizing pulses are shown in Fig. 14 (I–J and K–L). There was a progressive increase in magnitude and in time constant of the potential deflections during the time course of the pacemaker potential. Assuming C_m to remain constant, these data indicate that R_m is progressively increasing during the time course of V_p. No attempt was made to quantitate the change in R_m.

DISCUSSION

Biological application of the DC bridge technique to nerve electrophysiology (whereby one microelectrode simultaneously passes current and records transmembrane potentials) was originated by Bishop (3) and later used by Araki and Otani (1) and by Frank and Fuortes (12). More recently, Nagai and Prosser (27) and Ushiyama and Brooks (39) applied the technique to smooth and cardiac muscles, respectively; the latter investigators measured

thresholds, safety factor for conduction, break-excitation, and strength-duration curves of single cells. Some investigators claim that the bridge technique is not suitable because of fluctuations in resistance of the microelectrode during impalements and during passage of current (*e.g.*, reference 38). On the other hand, the present results clearly show that DC and AC bridge techniques can be successfully applied to a study of the electrophysiology of cardiac cells.

TABLE II

SUMMARY OF ELECTRICAL PARAMETERS OF TRYPSIN-DISPERSED CULTURED CHICK HEART CELLS (35°C)

Resting potential	59.0±1.2 mv (40–84 mv)
Action potential	71.2±1.5 mv (40–108 mv)
Rate of depolarization	1–10 v/sec.
Duration	150–500 msec.
Plateau	About 10 per cent of cells
Rate of beating	0–130/min.
Positive after-potential	0–20 mv
Pacemaker potential	0–15 mv (0–20 mv/sec.)
Prepotentials	Steps in rising phase
R_{cell}	12±0.9 megohms (mean of several methods)
R_m	480 ohm-cm²
C_{cell}	800 picofarads (measured, 840, calculated, 760)
C_m	20 μ farads/cm²
T_m	9.6 msec. (calculated, 10.1, measured, 9.1)
$[Na^+]_i$	16 mM*
$[K^+]_i$	186 mM*
E_{Na}	58 mv ($[Na]_o$ = 140)‡
E_K	−98 mv ($[K]_o$ = 4.5)‡
Na^+ efflux	14.2 pmole/cm² sec. ($t_{1/2}$ for washout of 1.17 min.)*
K^+ efflux	10.1 pmole/cm² sec. ($t_{1/2}$ for washout of 19.2 min.)*

* Data taken from Burrows and Lamb (5).

‡ Calculated diffusion potentials in our culture medium (145 mM Na^+, 4.5mM K^+). Assuming a steady resting potential of 70 mv, the calculated chord conductance for Na^+ (g_{Na}) is about 0.012 mmho/cm² and that for K^+, 0.035 mmho/cm². Even with the assumption of a relatively large g_{Cl}, the calculated R_m is about one order of magnitude too large; it is likely that the estimate of E_K is high.

Cultured chick heart cells may be grouped into two broad categories (Table III) according to functional considerations: (*a*) driven and (*b*) non-driven cells. The driven cells consist of non-pacemaker and latent pacemaker cells. The non-driven cells consist of true pacemaker, dormant pacemaker, and dormant non-pacemaker cells. The non-pacemaker cells had a stable membrane potential during electrical diastole. Polarizing current (0 to 4 nanoamp) had no effect on the frequency of discharge (or on the driving

frequency) of non-pacemaker cells and often had no effect on the frequency of latent pacemaker cells; however, in true and in dormant pacemaker cells, depolarizing current increased and hyperpolarizing current decreased the frequency of discharge. Similar results were obtained by Trautwein and Kassebaum (37) in pacemaker and potential pacemaker cells of sheep Purkinje fibers and rabbit sinus node by passage of DC current pulses through a second microelectrode. A true pacemaker is defined as a cell in which the pacemaker potential triggers the spike. A dormant pacemaker is a cell which

TABLE III

CLASSIFICATION OF CULTURED VENTRICULAR CELLS

	Type of cell				
	Non-driven			Driven	
	Dormant non-pacemaker	Dormant pacemaker	True pacemaker	Latent pacemaker	Non-pacemaker
Pacemaker potential	No	No (slight, irregular)	Yes	Yes	No
Driving prepotential	No	No	No	Yes	Yes
Second component	No	No	No	Often	Often
Overshoot	—	—	Greater	Lesser	—
Morphologically distinct	No	No	No	No	No
Positive after-potential	No (?)	Yes	Yes	Often	No (?)
Rate of firing:					
Without current	Zero	Zero	Low	High	High
Depolarizing current	No effect	Increase	Increase	Often no effect	No effect
Hyperpolarizing current	No effect	No observable effect	Decrease	Often no effect	No effect
Off-excitation	Often (?)	Yes	Yes	Yes	Often (?)
Positive off-potential	No (?)	Yes	Yes	Often (?)	No (?)

shows no action potentials, driving prepotentials, or pacemaker potentials (*i.e.*, has an uninterrupted steady resting potential) but which shows a repetitive discharge during the application of depolarizing current. A latent pacemaker is a cell which has pacemaker potentials but which is driven at a faster rate by other cells; V_p never reaches threshold and the action potential shows a prominent step or driving prepotential on the rising phase. The effect of polarizing current may be obscured if the driving frequency is sufficiently high. Some cells shifted back and forth between the categories of true pacemaker and latent pacemaker; in the former condition, there were no steps on the rising phases (22). No distinction between pacemaker and non-pacemaker cells was apparent on the basis of morphology and it was found that

any given cell shifted from time to time from one category into the other; *i.e.*, all cultured cells are probably capable of being pacemaker cells at one time or another. For example, visual observation of cells a few hours after culture showed up to 90 per cent of all isolated cells beating independently of one another (22). In addition, 60 to 70 per cent of all impaled cells were categorized as pacemaker cells.

In the present study, the magnitude of polarizing current, $\dot{V}_p$, and frequency of discharge were correlated. Progressive increments of depolarizing current increased $\dot{V}_p$ concomitantly with increased frequency of discharge, whereas hyperpolarizing current decreased $\dot{V}_p$ concomitantly with decreased frequency of discharge. Since R_m remained constant within limits of $\pm 4 \times 10^{-9}$ amp current, the change in $\dot{V}_p$ is a non-linear function of V_m and there is a narrow range of V_m in which $\dot{V}_p$ is most sensitive (Fig. 6). The relationship between frequency and $\dot{V}_p$ agrees with that calculated (dotted line in Fig. 7) assuming threshold depolarization of 10 mv and a constant refractory period of 0.4 sec. during which V_p is reset to zero. In a semilogarithmic plot, frequency was a linear function of log $\dot{V}_p$ between 1 and 30 mv/sec.; this curve had a steeper slope above 30 mv/sec. which can be accounted for on the basis of shortening of the action potential at frequencies above 60 impulses/min. (*cf.* reference 15). Crill *et al.* (8) reported a linear relationship between frequency and $\dot{V}_p$ for cultured chick heart cells (dashed line in Fig. 7); $\dot{V}_p$ ranged between 6 and 125 mv/sec. and frequency, 56 and 390 beats/min. There is reasonable agreement at low values of $\dot{V}_p$ and the discrepancy at high values may be partially accounted for by the difficulty of making accurate measurements.

The linear relationship between spike magnitude and intensity of polarizing current in pacemaker and non-pacemaker cells indicates that diastolic R_m remained constant (*i.e.*, no rectification) between $\pm 4 \times 10^{-9}$ amp. Crill *et al.* (8) and Trautwein and Kassebaum (37) found pronounced changes in spike magnitude as a function of polarizing current. In marked contrast, Johnson and Tille (21) found that in one type of rabbit ventricular cell, the amplitude (but not the rate of depolarization) of the action potential was rather insensitive to polarizing current (about ± 0.8 μamp); in a second type of ventricular cell, the action potential amplitude was quite sensitive to polarizing current (about -0.3 to $+0.02$ μamp). Even though the current and voltage microelectrodes were stated to be only 0.5 μ apart, the large resistive coupling between the electrodes made it impossible to measure the changes in resting potential. Likewise, Trautwein and Kassebaum (37), to attain similar changes in magnitude and frequency of action potentials, and Woodbury and Crill (43) to attain similar changes in resting potential, used over 100-fold more current than that used in the present study. In smooth muscle, excessive depolarizations abolished the action potentials and

left only irregular membrane oscillations as were found in the present study (27). If spike height is a function of V_m, the finding of an average change in spike magnitude of 22 per cent per 1×10^{-9} amp predicts a cell resistance of 12 to 16 MΩ (assuming a mean action potential of 72 mv). This indirect estimate for R_{cell} agrees closely with the mean value of 13 ± 1.2 MΩ obtained directly from voltage/current curves (Fig. 13). The calculated specific membrane resistance (R_m) of 480 Ω-cm² (Table II) is low compared to other values reported for cardiac muscle (40). For smooth muscle, 560 Ω-cm² has been calculated using a measured cell resistance of 69 MΩ (27). There was no substantial rectification between changes in V_m of ±30 mv. In addition, rectification has not been observed during the cardiac plateau by Johnson and Tille (*cf.* reference 21) who concluded that g_K was voltage-independent; assuming a space constant of 1 mm and a two dimensional syncytium, Noble (28) calculated that rectification would not be observed. Weidmann (41) found no evidence for delayed rectification in Purkinje fibers. Hutter and Noble (18) found rectification in sheep Purkinje fibers bathed in Na^+-free medium; resistance increased with depolarization (suggestive of a decrease in g_K) and decreased with hyperpolarization. Nagai and Prosser (27) found some rectification in smooth muscle upon depolarization but not upon hyperpolarization. The membrane specific capacitance (C_m), using 800 pf for C_{cell}, is 20 μf/cm² (Table II). This value compares closely with that calculated from the measured mean T_m of 9.1 msec. and from the mean resistance of 480 Ω-cm². Reported values of T_m include: 35 msec. for cultured chick heart cells (8), 19.5 msec. for ungulate Purkinje fibers (40), less than 1 msec. for rabbit ventricular fibers (20), 6.7 msec. for frog atrial fibers (38), and 31 msec. for smooth muscle (27).

A gradual decrease in K^+ conductance has been most widely accepted as the mechanism for the development of the V_p and may be subdivided into two classes (*cf.* references 10, 15, 29, 37, 41): (*a*) The decreased K^+ conductance may be a separate electrogenic process, perhaps related to the electrogenesis of the cardiac plateau (41, 42). (*b*) The decreased K^+ conductance may be a gradual return to normal following an increased K^+ conductance responsible for repolarization and for the positive after-potential (10); *i.e.*, the V_p may be considered as the termination of the positive after-potential. The qualitative finding in the present study of an increase in R_m and T_m during the pacemaker potential is in agreement with similar findings reported by Dudel and Trautwein (10) and Trautwein and Kassebaum (37); they concluded that V_p was produced by a progressive fall in g_K along with a constant, but relatively high, g_{Na}. During diastole (following a regenerative repolarization) a voltage-dependent, and to a lesser extent time-dependent, reduction in g_K produces a pacemaker potential; the diastolic g_{Na} was presumed to be large on the basis of hyperpolarization produced in Na^+-free

media (37). In contrast to such a mechanism, Carmeliet (6) suggested that V_p in sheep Purkinje cells is produced by an increased g_{Cl} resulting in a net outward flow of Cl^- ions (*cf.* reference 9). In analysis of the mechanism for the development of V_p, consideration must be given to the following additional facts (*cf.* reference 15): (*a*) Pacemaker cells (including visceral smooth muscle) generally have high Na^+, high Cl^-, and low K^+ concentrations compared to non-pacemaker cells (*cf.* references 9, 26). (*b*) $\dot{V}_p$ is markedly affected by temperature, acetylcholine, norepinephrine, and by the external K^+ concentration. (*c*) The acetylcholine system has been implicated in pacemaker activity (26). (*d*) Repetitive discharge and pacemaker potentials can be produced by constant current pulses in nerve (13) and skeletal muscle (2), by reduced extracellular Ca^{++} concentration in squid axon (19) and skeletal muscle (4, 36), by denervation of adult skeletal muscle (24), and by culturing of embryonic chick skeletal muscle (24).

The only requirement for a positive off-potential on the cessation of depolarizing pulses appeared to be that the cell have a natural positive after-potential. It is likely that all pacemaker cells exhibited positive after-potentials. The magnitude of the positive off-potential was a function of the intensity of current and was probably a function of the difference between the resting potential and E_K. If threshold intensity or above, hyperpolarizing current led to the phenomenon of off-excitation (*cf.* reference 8). It would thus appear that the positive off-potential and off-excitation are related to the well known phenomena of post-cathodal depression and post-anodal enhancement of excitability. Post-cathodal depression can be accounted for by a sustained decrease in h factor (Na inactivation) which decays relatively slowly following cessation of the depolarizing pulse (*cf.* reference 14). There is thus a relatively large K^+ fractional conductance after the current-off which leads to hyperpolarization towards E_K. One explanation for the early positive after-potential in nerve, was in terms of conductance changes, namely an increased g_K which persists after repolarization is complete (14). However, other explanations (*cf.* reference 31) have also been invoked because of the following characteristics of late positive after-potentials in nerve: (*a*) they become greatly enhanced in magnitude and duration following repetitive impulses (post-tetanic hyperpolarization); (*b*) they are diminished by cooling, anoxia, and metabolic poisons (dinitrophenol); (*c*) they are diminished by cardiac glycosides concomitant with suppression of the extra oxygen uptake of active nerve; (*d*) they are increased in amplitude and duration by 0.5 mM Ni^{++} concomitant with an increased oxygen uptake (7); (*e*) they are diminished by Na^+ replacement with Li^+. Therefore, the other explanations proposed center around enhanced Na-K active transport: (*a*) an enhanced electrogenic Na^+ pump (7, 35) and (*b*) a greater E_K (*cf.* reference 31). The latter may

result from enhanced pumping action of a non-electrogenic Na-K coupled pump combined with a diffusion lag between the bulk extracellular solution and that just outside of the cell membrane; thus, E_K is increased mainly because of decreased $[K^+]_o$. However, if a pump mechanism were responsible for the positive off-potential, one would expect a progressive hyperpolarization during the current pulse; instead the change in V_m remained steady during the entire current-clamp period. Similarly, the positive off-potential cannot be due to electrophoresis of K^+ into the cell from the microelectrode, thereby increasing E_K. Furthermore, increased $[K^+]_i$ levels expected by electrophoresis, even assuming no K^+ efflux, cannot account for the observed magnitude of the positive off-potentials, and positive off-potentials were produced using microelectrodes filled with 3 M NaCl. If one assumes that the rate of the sodium pump is controlled by the intracellular Na^+ concentration, neither an electrogenic nor a non-electrogenic Na pump is likely to be the cause of the off-potential. In preliminary experiments, 0.5 mM Ni^{++} appears to have no significant effect on the positive after-potentials or off-potentials of cultured heart cells.

The present experiments with cultured heart cells suggest that there is a transmembrane resting potential across each membrane of the intercalated disc; *i.e.*, the fluid in the junctional gap between the disc membranes is extracellular fluid. Single cultured cells beat independently of each other; when the cells grew together physically they usually beat synchronously. Pushing together of two independently beating cultured cells did not cause them to synchronize; thus, such artificial ephapse experiments do not result in electrotonic interaction. However, it is conceivable that with a natural contact between the two cells during growth of the culture, the junctional membranes may become low resistance or may become specialized for chemical synaptic interaction. The finding that a second cell of a naturally joined doublet possessed a substantial resting potential at a time when its adjoining neighbor, across a previously functional junction, was entirely depolarized indicates that there is a sharp discontinuity of potential between the myoplasm of two adjoining cells. The presence of this potential does not necessarily mean that the disc membranes are high resistance, but it does make this possibility more likely. Several lines of evidence in the past have suggested non-electrotonic interaction between adjoining heart cells and it was concluded that the intercalated discs were high resistance (32–34).

Prepotentials have been found previously in cultured chick embryonic cardiac cells (22) as well as in adult cardiac cells (16, 34, 37). In studies on cardiac fibrillation induced by hypertonic solution, Mashiba (25) concluded that slow junction potential components represented interaction of adjacent cells (*cf.* reference 17). Evidence from the present study that the prepotential

represents the transmission of excitation from adjoining cells was obtained by correlation of the contractions with the electrical activity of the impaled cell. In all instances, a spike was accompanied by a contraction of the impaled cell and its neighboring cells, whereas the prepotential was not accompanied by a contraction of the impaled cell. Thus, in many cases transmission of excitation failed and such failures were increased under conditions of depressed excitability produced by hyperpolarizing current and decreased with enhanced excitability produced by depolarizing current. The shapes of the prepotentials were similar to what one would expect if they represented postsynaptic potentials. The spontaneous frequency of discharge was often higher in driven (up to 130 impulses/min.) than in true pacemaker cells. It is likely that high driving frequencies were obtained by action of two or more pacemaker cells upon the impaled cell. Second components of the intracellular responses from driven cells occasionally occurred on the repolarizing phase of the action potentials and may represent a second driving prepotential because they often occurred at a slightly different rate than the spikes (22, 34). Further evidence for two driving prepotentials acting upon one cell is the presence of small and large prepotentials in the same cell. The difference in the magnitudes of the small and large prepotentials and in the effect of polarizing current upon their magnitudes may be explainable on the basis of the distance from the junction to the recording microelectrode. Thus, the large prepotentials would be recorded when the microelectrode was close to a junction. Polarizing current should only affect the large prepotential because V_m would not be greatly altered at a distant junction (if the space constant were short). The shape of many cultured cells was such that a functional junction could have been at the end of a long, narrow cell process. Postsynaptic potentials (chemical transmission) can be distinguished from ephaptic potentials (purely electrical transmission) on the basis of the effect of polarizing currents: ephaptic potentials should be unaffected by polarizing currents (if R_m remains constant), whereas excitatory postsynaptic potentials should become enhanced with hyperpolarization and diminished with depolarization. Therefore, the behavior of the large prepotential is consistent with the hypothesis that it represents a chemical post-synaptic potential.

The technical assistance of John Egna in the preparation of the cultured heart cells is gratefully acknowledged; Jerold Lower made valuable suggestions related to the design of the AC bridge circuit.

This work was supported by grants from the Cleveland Area Heart Society and from the Public Health Service (H-5087).

Dr. Sperelakis is an Established Investigator of the American Heart Association.

Received for publication, October 31, 1963.

REFERENCES

1. ARAKI, T., and OTANI, T., Response of single motoneurons to direct stimulation in toad's spinal cord, *J. Neurophysiol.*, 1955, **18**, 472.
2. BENOIT, P. H., CORABOEUF, E., and ETZENSPERGER, J., Données microphysiologiques sur la fibre musculaire striée, *Colloq. Internat. Centre Nat. Recherche Sc. Paris*, Juillet 19–23, 1955.
3. BISHOP, G. H., The form of the record of the action potential of vertebrate nerve at the stimulated region, *Am. J. Physiol.*, 1927, **82**, 462.
4. BÜLBRING, E., Similarity between the behavior of striated muscle deficient in calcium and that of certain smooth muscle, *J. Physiol.*, 1955, **129**, 22P.
5. BURROWS, R., and LAMB, J. F., Sodium and potassium fluxes in cells cultured from chick embryo heart muscle, *J. Physiol.*, 1962, **162**, 510.
6. CARMELIET, E. E., Chloride ions and the membrane potential of Purkinje fibers, *J. Physiol.*, 1961, **156**, 375.
7. CONNELLY, C. M., Metabolic and electrochemical events associated with recovery from activity, *Proc. XXII Internat. Cong. Physiol. Sc.*, Leiden, 1962, 600.
8. CRILL, W. E., RUMERY, R. E., and WOODBURY, J. W., Effects of membrane current on transmembrane potentials of cultured chick embryo heart cells, *Am. J. Physiol.*, 1959, **197**, 733.
9. DE MELLO, W. C., Role of chloride ions in cardiac action and pacemaker potentials, *Am. J. Physiol.*, 1963, **205**, 567.
10. DUDEL, J., and TRAUTWEIN, W., Der Mechnismus der automatischen rhythmischen Impulsbildung der Herzmuskelfaser, *Arch. ges. Physiol.*, 1958, **267**, 553.
11. FÄNGE, R., PERSSON, H., and THESLEFF, S., Electrophysiologic and pharmacological observations on trypsin-disintegrated embryonic chick hearts cultured *in vitro*, *Acta Physiol. Scand.*, 1956, **38**, 173.
12. FRANK, K., and FUORTES, M. G. F., Stimulation of spinal motoneurones with intracellular electrodes, *J. Physiol.*, 1956, **134**, 451.
13. HODGKIN, A. L., The local electric changes associated with repetitive action in a non-medullated axon, *J. Physiol.*, 1948, **107**, 165.
14. HODGKIN, A. L., Ionic movements and electrical activity in giant nerve fibers, *Proc. Roy. Soc. London, Series B*, 1957, **148**, 1.
15. HOFFMAN, B. F., and CRANEFIELD, P. F., Electrophysiology of the Heart, New York, McGraw-Hill Book Company, 1960.
16. HOSHIKO, T., and SPERELAKIS, N., Prepotentials and unidirectional propagation in myocardium, *Am. J. Physiol.*, 1961, **201**, 873.
17. HOSHIKO, T., and SPERELAKIS, N., Components of the cardiac action potential, *Am. J. Physiol.*, 1962, **203**, 258.
18. HUTTER, O. F., and NOBLE, D., Rectifying properties of cardiac muscle, *Nature*, 1960, **188**, 495.
19. HUXLEY, A. F., Ion movements during nerve activity, *Ann. New York Acad. Sc.*, 1959, **81**, 221.

20. JOHNSON, E. A., and TILLE, J., Investigations of the electrical properties of cardiac muscle fibers with the aid of intracellular double-barrelled electrodes, *J. Gen. Physiol.*, 1961, **44**, 443.

21. JOHNSON, E. A., and TILLE, J., Evidence for independence of voltage of the membrane conductance of rabbit ventricular fibers, *Nature*, 1961, **192**, 663.

22. LEHMKUHL, D., and SPERELAKIS, N., Transmembrane potentials of trypsin-dispersed chick heart cells cultured *in vitro*, *Am. J. Physiol.*, 1963, **205**, 1213.

23. LETTVIN, J. Y., HOWLAND, B., and GESTELAND, R. C., Footnotes on a head-stage, *IRE Tr. Med. Electron.*, 1958, **10**, 26.

24. LI, C. L., ENGEL, K., and KLATZO, I., Some properties of cultured chick skeletal muscle with particular reference to fibrillation potential, *J. Cell and Comp. Physiol.*, 1959, **53**, 421.

25. MASHIBA, H., Studies on fibrillation; ordinary action potential and interaction potential, *Japan. Heart J.*, 1961, **2**, 487.

26. MAZEL, P., and HOLLAND, W. C., Acetylcholine and electrolyte metabolism in the various chambers of the frog and turtle heart, *Circulation Research*, 1958, **6**, 684.

27. NAGAI, T., and PROSSER, C. L., Electrical parameters of smooth muscle cells, *Am. J. Physiol.*, 1963, **204**, 915.

28. NOBLE, D., The voltage dependence of the cardiac membrane conductance, *Biophysic. J.*, 1962, **2**, 381.

29. NOBLE, D., A modification of the Hodgkin-Huxley equations applicable to Purkinje fiber action and pacemaker potentials, *J. Physiol.*, 1962, **160**, 317.

30. PUCK, T. T., CIECIURA, S. J., and ROBINSON, A., Genetics of somatic mammalian cells. III. Long-term cultivation of euploid cells from human and animal subjects, *J. Exp. Med.*, 1958, **108**, 945.

31. RITCHIE, J. M., Possible mechanisms underlying production of after-potential in nerve fibers, *in* Biophysics of Physiological and Pharmacological Actions, (A. M. Shanes, editor), Washington, The American Association for the Advancement of Science Symposium, 1961.

32. SPERELAKIS, N., Additional evidence for high-resistance intercalated discs in the myocardium, *Circulation Research*, 1963, **12**, 676.

33. SPERELAKIS, N., and HOSHIKO, T., Electrical impedance of cardiac muscle, *Circulation Research*, 1961, **9**, 1280.

34. SPERELAKIS, N., HOSHIKO, T., KELLER, R. F., JR., and BERNE, R. M., Intracellular and external recording from frog ventricular fibers during hypertonic perfusion, *Am. J. Physiol.*, 1960, **198**, 135.

35. STRAUB, R. W., Mechanism of post-tetanic hyperpolarization, *Proc. XXII Internat. Cong. Physiol. Sc.*, Leiden, 1962, 598.

36. TAMAI, T., ABE, Y., and GOTO, M., Interaction between adjoining fibers in the fibrillating skeletal muscle of the frog, *Japan. J. Physiol.*, 1961, **11**, 346.

37. TRAUTWEIN, W., and KASSEBAUM, D. G., On the mechanism of spontaneous impulse generation in the pacemaker of the heart, *J. Gen. Physiol.*, 1961, **45**, 317.

38. TRAUTWEIN, W., KUFFLER, S. W., and EDWARDS, C., Changes in membrane characteristics of heart muscle during inhibition, *J. Gen. Physiol.*, 1956, **40**, 135.
39. USHIYAMA, J., and BROOKS, C. McC., Intracellular stimulation and recording from single cardiac cells, *Am. J. Cardiol.*, 1962, **10**, 688.
40. WEIDMANN, S., The electrical constants of Purkinje fibers, *J. Physiol.*, 1952, **118**, 348.
41. WEIDMANN, S., Elektrophysiologie der Herzmuskelfaser, Bern, Hans Huber, 1956.
42. WOODBURY, J. W., Voltage and time-dependent membrane conductance changes in cardiac cells, *in* Biophysics of Physiological and Pharmacological Actions, (A. M. Shanes, editor), Washington, The American Association for the Advancement of Science Symposium, 1961, 501.
43. WOODBURY, J. W., and CRILL, W. E., On the problem of impulse conduction in the atrium, *in* Nervous Inhibition, (E. Florey, editor), New York, Pergamon Press, Inc., 1961, 124.